Predictions of the strange partner of T_{cc} in the quark delocalization color screening model

Xuejie Liu,[1,†] Dianyong Chen,[2,4,*] Hongxia Huang,[3,‡] and Jialun Ping[3,§]

[1]School of Physics, Henan Normal University, Xinxiang 453007, People's Republic of China
[2]School of Physics, Southeast University, Nanjing 210094, People's Republic of China
[3]Department of Physics, Nanjing Normal University, Nanjing 210023, People's Republic of China
[4]Lanzhou Center for Theoretical Physics, Lanzhou University, Lanzhou 730000, People's Republic of China

(Received 15 September 2023; accepted 16 February 2024; published 11 March 2024)

Inspired by the detection of T_{cc} tetraquark state by LHCb Collaboration, we perform a systemical investigation of the low-lying doubly heavy charm tetraquark states with strangeness in the quark delocalization color screening model in the present work. Two kinds of configurations, the meson-meson configuration and diquark-antidiquark configuration, are considered in the calculation. Our estimations indicate that the coupled channel effects play important role in the multiquark system, and a bound state with $J^P = 1^+$ and a resonance state with $J^P = 0^+$ have been predicted. The mass of the bound state is evaluated to be (3971–3975) MeV, while the mass and width of the resonance are determined to be (4113–4114) MeV and (14.3–16.1) MeV, respectively.

DOI: 10.1103/PhysRevD.109.054021

I. INTRODUCTION

In the recent two decades, an increasing number of charmoniumlike states have been observed experimentally, which provide a good opportunity of searching for multiquark states. As the first confirmed charmoniumlike state, $Z_c(3900)$ was first observed in the year of 2013 by the BESIII [1] and Belle [2] Collaborations in the $\pi^+ J/\psi$ invariant mass spectrum of the process $e^+e^- \to \pi^+\pi^- J/\psi$ at a center of mass energy of 4.26 GeV, and then the authors of Ref. [3] further confirmed the existence of $Z_c(3900)$ by using the data sample collected by CLEO-c detector in the same process but at $\sqrt{s} = 4.170$ GeV. The partial wave analysis of the process $e^+e^- \to \pi^+\pi^- J/\psi$ with the data sample accumulated at $\sqrt{s} = 4.23$ and 4.26 GeV indicated that the spin and parity of the $Z_c(3900)^{\pm}$ state are 1^+ [4]. The observations indicate that such a new particle cannot be simply interpreted in the conventional quark-antiquark and three-quark schemes. Thus, some exotic interpretations, such as tetraquark state [5–8], hadronic molecular state [9–17], have been proposed. Besides the resonance interpretations, $Z_c(3900)$ has also been considered as the kinematic effects [18–23], which indicated that $Z_c(3900)$ was not a genuine resonance.

In the resonance frame, the quark component of $Z_c(3900)$ is $c\bar{c}q\bar{q}$. The flavor independence of the strong interactions naturally indicates the possible existence of the strange partner of $Z_c(3900)$, whose quark components are $c\bar{c}s\bar{q}$. Such kind of charmoniumlike states with strangeness have been predicted theoretically in various model, such as tetraquark scenarios [24,25], hadronic molecular model [26,27], the hadro-quarkonium model [25] and initial single chiral particle emission mechanism [28]. In the year of 2020, the BES III Collaboration observed a new states named $Z_{cs}(3985)$ in the K^+ recoil mass distributions of the process $e^+e^- \to K^+ D_s^- D^{*0}/K^+ D_s^{*-} D^0$ [29]. Later on, the LHCb Collaboration reported their observation of two exotic structures, $Z_{cs}(4000)$ and $Z_{cs}(4220)$, in the $J/\psi K^+$ invariant mass spectrum of the $B^+ \to J/\psi\phi K^+$ decay in 2021 [30]. Since the observed masses of $Z_{cs}(3985)$ and $Z_{cs}(4000)$ were similar, these two states may be considered as the same one (hereinafter, we use $Z_{cs}(3985)$ to refer to this state). It is interesting to notice that $Z_c(3900)$ is located in the vicinity of the $D^*\bar{D}$ threshold, while $Z_{cs}(3985)$ is close to $D_s^*\bar{D}$ threshold, thus one can consider $Z_{cs}(3985)$ as a strange partner of $Z_c(3900)$. Consequently, the hadronic molecular [31–40], compact tetraquark [41–43] and hadro-quarkonium [25] scenarios have been proposed to decode the nature of $Z_{cs}(3985)$.

*Corresponding author: chendy@seu.edu.cn
†1830592517@qq.com
‡hxhuang@njnu.edu.cn
§jlping@njnu.edu.cn

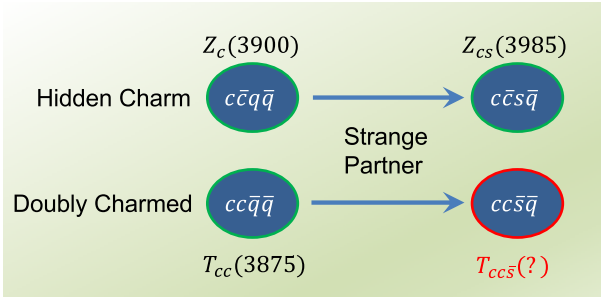

FIG. 1. The similarity of the hidden charm and doubly charmed states. Hereinafter, $T_{cc\bar{s}}$ is used to refer the doubly charmed state with strangeness.

In the naive multiquark scenario, if there are multiquark states composed of $c\bar{c}q\bar{q}$, the states composed of $cc\bar{q}\,\bar{q}$ are also expected to exist and have been considered to be the molecular $D^{*+}D^0$ states [44–60], and compact states [61–63]. Recently, the LHCb Collaboration reported the observation of the first doubly charmed tetraquark state $T_{cc}^+(3875)$ in the $D^0D^0\pi^+$ mass spectrum just below the $D^{*+}D^0$ mass threshold [64,65] with $I(J^P) = 1(1^+)$. As indicated in Fig. 1, the quark components of $T_{cc}(3875)$ are $cc\bar{q}\,\bar{q}$, which indicate that $T_{cc}(3875)$ could be a good candidate of compact tetraquark state. In Refs. [61,62], the authors investigated the mass spectrum of the S–wave doubly heavy tetraquark states $QQ\bar{q}\,\bar{q}$ based on the improved chromomagnetic interaction model and found a stable $cc\bar{u}\,\bar{d}$ tetraquark state with $I(J^P) = 0(1^+)$ below the $D^{*+}D^0$ threshold, which is well consistent with the observed $T_{cc}^+(3875)$. Moreover, the QCD sum rule estimation in Ref. [63] also supported the compact tetraquark interpretation. In addition, the observed mass of $T_{cc}^+(3875)$ is only several hundred keV below the threshold of D^0D^{*+}, which imply that $T_{cc}^+(3875)$ could be interpreted as a shallow molecular state composed of D^0D^{*+} + H.c. Further estimations by using the quark models [44–48,57–59], QCD sum rules [49–51], heavy quark symmetry [52–54,60] and Bethe-Salpeter equations [55,56] indicated that $T_{cc}^+(3875)$ could be a good candidate of D^0D^{*+} + H.c. molecular state.

Similar to the relation between $Z_{cs}(3985)$ and $Z_c(3900)$, one can expect the existence of the strange partner of $T_{cc}(3875)$, i.e., the tetraquark states composed of $cc\bar{q}\,\bar{s}$. Actually, before the observation of $T_{cc}^+(3875)$, the Lattice QCD estimations in Ref. [66] predicted that the $T_{cc\bar{s}}$ state with $J^P = 1^+$ was about 10 MeV below the threshold of $D^+D_s^{*-}$, while the estimations by using the heavy quark symmetry in Ref. [67] found its mass to be about 180 MeV above the corresponding threshold. In Ref. [68], the predicted $T_{cc\bar{s}}$ tetraquark state with $J^P = 1^+$ was below the threshold of $D^+D_s^{*-}$, while those with $J^P = 0^+$ and 2^+ were both above the corresponding thresholds. After the observation of T_{cc}^+, the authors in Ref. [60] took advantage of the experimental information on the binding energy of T_{cc}^+ to fix the cutoff regulator of the loops in the Bethe-Salapeter equation and a $D_s^*D^*$ bound state with $J^P = 1^+$ was predicted. Besides, the color-magnetic model estimations in Ref. [69] implied that both T_{cc}^+ and $T_{cc\bar{s}}^+$ system could be stable against the strong interactions. However, the state $T_{cc\bar{s}}^+$ was not found in the quark model but if the mixing of S–D wave was taken into account, this state may be obtained [59]. As mentioned above, theorists have not reach an agreement on the existence of $T_{cc\bar{s}}$ tetraquark states. In the present work, we perform a system estimations of $T_{cc\bar{s}}$ system by using the quark delocalization color screening model (QDCSM) in an attempt to further explore the existence of the possible bounded and resonant states in the $T_{cc\bar{s}}$ system.

This paper is organized as follows. After the introduction, the details of the QDCSM and resonating group method (RGM) are presented in Sec. II. Our numerical results and the related discussions for $T_{cc\bar{s}}$ system are given in Sec. III, and the last section is devoted to a short summary.

II. QUARK DELOCALIZATION COLOR SCREENING MODEL AND THE RESONANTING GROUP METHOD

A. Quark delocalization color screening model

The QDCSM is an extension of the native quark cluster model [70–73] and also developed with aim of addressing multiquark systems. For the tetraquark system, the Hamiltonian reads,

$$H = \sum_{i=1}^{4}\left(m_i + \frac{\boldsymbol{p}_i^2}{2m_i}\right) - T_{CM} + \sum_{j>i=1}^{4} V(r_{ij}), \quad (1)$$

where T_{CM} is the center-of-mass kinetic energy, who is usually subtracted without losing generality since we mainly focus on the internal relative motions of the multiquark system. The interplay is two body potential, which includes color-confining potential $V_{\rm CON}$, one-gluon exchange potential $V_{\rm OGE}$, and the potential results from Goldstone-boson exchange, V_χ, i.e.,

$$V(r_{ij}) = V_{\rm CON}(r_{ij}) + V_{\rm OGE}(r_{ij}) + V_\chi(r_{ij}). \quad (2)$$

In the present work, we focus on the S–wave low-lying positive $T_{cc\bar{s}}$ tetraquark system with positive parity. In this case, the spin-orbit and tensor interactions vanish and the potential $V_{\rm OGE}(r_{ij})$ becomes,

$$V_{\rm OGE}(r_{ij}) = \frac{1}{4}\alpha_s^{q_iq_j}\boldsymbol{\lambda}_i^c\cdot\boldsymbol{\lambda}_j^c \times\left[\frac{1}{r_{ij}} - \frac{\pi}{2}\delta(\boldsymbol{r}_{ij})\left(\frac{1}{m_i^2}+\frac{1}{m_j^2}+\frac{4\boldsymbol{\sigma}_i\cdot\boldsymbol{\sigma}_j}{3m_im_j}\right)\right], \quad (3)$$

where m_i is the quark mass, $\boldsymbol{\sigma}_i$ and $\boldsymbol{\lambda}_i^c$ are the Pauli matrices and SU(3) color matrices, respectively. The $\alpha_s^{q_iq_j}$ is the quark-gluon coupling constant, which offers a consistent description of mesons from light to heavy-quark sector. The values of α_{ij} are associated with the quark flavors and in the present work they are fixed by reproducing the mass difference of the low-lying mesons with $S = 0$ and $S = 1$.

The confining potential $V_{\rm CON}(r_{ij})$ is,

$$V_{\rm CON}(r_{ij}) = -a_c\boldsymbol{\lambda}_i^c\cdot\boldsymbol{\lambda}_j^c\left[f(r_{ij}) + V_{0_{q_iq_j}}\right], \tag{4}$$

where the $V_{0_{q_iq_j}}$ is determined by the mass differences of the theoretical estimations and experimental measurement of each kind of meson, which is also quark flavor related parameter. In the QDCSM, the function $f(r_{ij})$ is defined as,

$$f(r_{ij}) = \begin{cases} r_{ij}^2 & \text{if } i,j \text{ occur in the same cluster,} \\ \frac{1-e^{-\mu_{ij}r_{ij}^2}}{\mu_{ij}} & \text{if } i,j \text{ occur in different cluster,} \end{cases} \tag{5}$$

where the color screening parameter μ_{ij} relevant to the light quarks can be determined by fitting the deuteron properties, NN and NY scattering phase shifts [74–76], which are $\mu_{qq} = 0.45$, $\mu_{qs} = 0.19$, and $\mu_{ss} = 0.08$. The parameter μ_{ij} satisfy the relation $\mu_{qs}^2 = \mu_{qq}\mu_{ss}$, where q represents u or d quark. When extending to the heavy-quark case, we found that the dependence of the parameter μ_{cc} is rather weak in the calculation of the spectrum of P_c states by taking the value of μ_{cc} from 10^{-4} to 10^{-2} fm^{-2} [77]. Moreover, when μ_{ij} is rather small, the exponential function can be approximated to be,

$$e^{-\mu_{ij}r_{ij}^2} = 1 - \mu_{ij}r_{ij}^2 + \mathcal{O}(\mu_{ij}^2r_{ij}^4). \tag{6}$$

in the small r region. Accordingly, the confinement potential between two clusters is approximated to be,

$$\begin{aligned} V_{\rm CON}(r_{ij}) &= -a_c\boldsymbol{\lambda}_i^c\cdot\boldsymbol{\lambda}_j^c\left(\frac{1-e^{-\mu_{ij}r_{ij}^2}}{\mu_{ij}} + V_{0_{ij}}\right) \\ &\approx -a_c\boldsymbol{\lambda}_i^c\cdot\boldsymbol{\lambda}_j^c(r_{ij}^2 + V_{0_{ij}}), \end{aligned} \tag{7}$$

which is the same with the expression of two quarks in the same cluster. Thus, when the value of the μ_{ij} is very small, the screened confinement will return to the quadratic form, which is why the results are insensitive to the value of μ_{cc}. So in the present work, we take $\mu_{cc} = 0.01$ fm^{-2}. Then μ_{sc} and μ_{uc} are obtained by the relation $\mu_{sc}^2 = \mu_{ss}\mu_{cc}$ and $\mu_{uc}^2 = \mu_{uu}\mu_{cc}$, respectively.

The Goldstone-boson exchange interactions between light quarks appear because the dynamical breaking of chiral symmetry. For the $T_{cc\bar{s}}$ system, the π exchange interaction vanishes because there is no unflavor quark pair in the tetraquark state, and then the concrete form of the Goldstone-boson exchange potential becomes,

$$\begin{aligned} V_{ij}^{\chi} &= V_K(\boldsymbol{r}_{ij})\sum_{a=4}^{7}\lambda_i^a\cdot\lambda_j^a \\ &\quad + V_\eta(\boldsymbol{r}_{ij})\left[(\lambda_i^8\cdot\lambda_j^8)\cos\theta_P - (\lambda_i^0\cdot\lambda_j^0)\sin\theta_P\right], \end{aligned} \tag{8}$$

with

$$\begin{aligned} V_\chi(\boldsymbol{r}_{ij}) &= \frac{g_{ch}^2}{4\pi}\frac{m_\chi^2}{12m_im_j}\frac{\Lambda_\chi^2}{\Lambda_\chi^2 - m_\chi^2}m_\chi \\ &\quad\times\left\{(\boldsymbol{\sigma}_i\cdot\boldsymbol{\sigma}_j)\left[Y(m_\chi r_{ij}) - \frac{\Lambda_\chi^3}{m_\chi^3}Y(\Lambda_\chi r_{ij})\right]\right\}, \\ \chi &= \{K,\eta\}, \end{aligned} \tag{9}$$

where $Y(x) = e^{-x}/x$ is the standard Yukawa function. The $\boldsymbol{\lambda^a}$ is the SU(3) flavor Gell-Mann matrix. The mass of the K and η meson is taken from the experimental value [78]. The chiral coupling constant, g_{ch}, is determined from the πNN coupling constant through,

$$\frac{g_{ch}^2}{4\pi} = \left(\frac{3}{5}\right)^2\frac{g_{\pi NN}^2}{4\pi}\frac{m_{u,d}^2}{m_N^2}, \tag{10}$$

where the SU(3) flavor symmetry only broken by the different masses of the light quarks. All the other model parameters are the same as the ones in Ref. [79], which were determined by reproducing the mass spectrum of the ground mesons. With three different sets of parameters, the authors of Ref. [79] extended this model to investigate the $c\bar{c}s\bar{s}$ tetraquark system, and they found that some charmoniumlike states could be interpreted as $c\bar{c}s\bar{s}$ tetraquark states. For the sake of completeness, we collect the relevant model parameters in Table I.[1]

In the QDCSM, the single-particle orbital wave functions in the ordinary quark cluster model are the left and right centered single Gaussian functions, which are,

$$\begin{aligned} \phi_\alpha(\boldsymbol{S_i}) &= \left(\frac{1}{\pi b^2}\right)^{\frac{3}{4}}e^{-\frac{(r_\alpha-\frac{1}{2}s_i)^2}{2b^2}}, \\ \phi_\beta(-\boldsymbol{S_i}) &= \left(\frac{1}{\pi b^2}\right)^{\frac{3}{4}}e^{-\frac{(r_\beta+\frac{1}{2}s_i)^2}{2b^2}}. \end{aligned} \tag{11}$$

The quark delocalization is realized by writing the single-particle orbital wave function as a linear combination of the left and right Gaussians, which are,

[1]As for the α_s^{cc}, it is determined by the mass difference of J/ψ and η_c. It should be noted that the coefficient of $\boldsymbol{\sigma}_i\cdot\boldsymbol{\sigma}_j$ is $\alpha_s^{cc}/(3m_c^2)$, since m_c is much larger than m_u and m_s, thus, we need a large α_s^{cc} to reproduce the mass splitting between J/ψ and η_c.

TABLE I. Three sets of model parameters involved in the present estimations.

	Parameters	QDCSM1	QDCSM2	QDCSM3
Quark mass	m_u(MeV)	313	313	313
	m_s(MeV)	536	536	536
	m_c(MeV)	1728	1728	1728
Confinement	b(fm)	0.29	0.3	0.315
	a_c(MeV fm^{-2})	101	101	101
	$V_{0_{uu}}$(MeV)	−2.3928	−2.2543	−2.0689
	$V_{0_{us}}$(MeV)	−1.9137	−1.7984	−1.6429
	$V_{0_{uc}}$(MeV)	−1.4175	−1.3231	−1.2052
	$V_{0_{ss}}$(MeV)	−1.3448	−1.2826	−1.2745
	$V_{0_{sc}}$(MeV)	−0.7642	−0.6739	−0.5452
	$V_{0_{cc}}$(MeV)	0.6063	0.7555	0.9829
OGE	α_s^{uu}	0.2292	0.2567	0.3019
	α_s^{us}	0.2655	0.2970	0.3484
	α_s^{uc}	0.3437	0.3805	0.4405
	α_s^{ss}	0.3856	0.3604	0.3360
	α_s^{sc}	0.5969	0.6608	0.7649
	α_s^{cc}	1.5101	1.6717	1.9353

$$\psi_\alpha(\boldsymbol{S_i},\epsilon) = (\phi_\alpha(\boldsymbol{S_i}) + \epsilon\phi_\alpha(-\boldsymbol{S_i}))/N(\epsilon),$$
$$\psi_\beta(-\boldsymbol{S_i},\epsilon) = (\phi_\beta(-\boldsymbol{S_i}) + \epsilon\phi_\beta(\boldsymbol{S_i}))/N(\epsilon),$$
$$N(\epsilon) = \sqrt{1+\epsilon^2+2\epsilon e^{-S_i^2/4b^2}}, \tag{12}$$

where the mixing parameter $\epsilon(\boldsymbol{S}_i)$ is not an adjusted one but is determined variationally by the dynamics of the multiquark system itself. This assumption allows the multiquark system to choose its favorable configuration in the interacting process. It has been used to explain the cross-over transition between the hadron phase[2] and the quark-gluon plasma phase [80–82]. Due to the effect of the mixing parameter $\epsilon(s_i)$, there is a certain probability for the quarks between the two clusters to run, which leads to the existence of color octet states for the two clusters. Therefore, this model also includes the hidden color channel effect, which is confirmed by Refs. [83,84].

B. The resonating group method

In the present work, the RGM is employed to carry out the dynamical calculation. When dealing with the two-cluster system in this method, one can only consider the relative motion between the clusters, while the two clusters

[2]The phase shift of NN interaction could be described with the formalisms with hadrons only. After including the pseudoscalar, vector, and scalar meson, especially the σ meson, the NN interaction has been well described. In Ref. [80], the authors concluded that the σ-meson exchange can be replaced by quark delocalization and color screening mechanism introduced by QDCSM by comparing the NN scattering and deuteron properties obtained by chiral quark model and QDCSM.

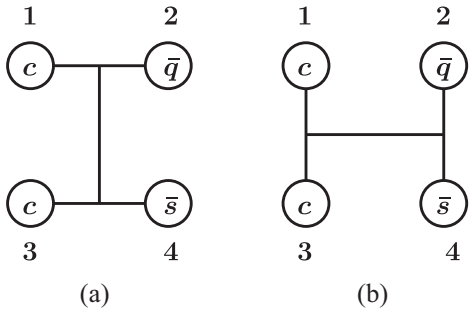

FIG. 2. The meson-meson configuration [diagram (a)] and diquark-antidiquark configuration [diagram (b)] in the $T_{cc\bar{s}}$ tetraquark system.

are frozen inside [85]. So the wave function of the $T_{cc\bar{s}}$ system can be constructed as,

$$\psi_{4q} = \mathcal{A}\left[[\psi_A(\boldsymbol{\rho}_A)\psi_B(\boldsymbol{\rho}_B)]^{[\sigma]IS} \otimes \chi_L(\mathbf{R})\right]^J, \tag{13}$$

where the symbol $\mathcal{A}$ is the antisymmetry operator, which is defined as

$$\mathcal{A} = 1 - P_{13}, \tag{14}$$

where the P_{13} indicates the exchange of the particle positions with numbers 1 and 3 from the Fig. 2. $[\sigma] = [222]$ gives the total color symmetry. The symbols I, S, L, and J represent flavor, spin, orbit angular momentum, and total angular momentum of $T_{cc\bar{s}}$ system, respectively. ψ_A and ψ_B are the wave functions of the two-quark cluster, which are,

$$\psi_A = \left(\frac{1}{2\pi b^2}\right)^{3/4} e^{-\boldsymbol{\rho}_A^2/(4b^2)}\eta_{I_A}S_A\chi_A^c,$$
$$\psi_B = \left(\frac{1}{2\pi b^2}\right)^{3/4} e^{-\boldsymbol{\rho}_B^2/(4b^2)}\eta_{I_B}S_B\chi_B^c, \tag{15}$$

where η_I, S, and χ represent the flavor, spin and internal color terms of the cluster wave functions, respectively. According to Fig. 2, we adopt different Jacobi coordinates for different diagrams. As for the meson-meson configuration in Fig. 2(a), the Jacobi coordinates are defined as,

$$\boldsymbol{\rho_A} = \boldsymbol{r}_{q_1} - \boldsymbol{r}_{\bar{q}_2}, \qquad \boldsymbol{\rho_B} = \boldsymbol{r}_{q_3} - \boldsymbol{r}_{\bar{q}_4},$$
$$\boldsymbol{R_A} = \frac{m_1\boldsymbol{r}_{q_1} + m_2\boldsymbol{r}_{\bar{q}_2}}{m_1+m_2},$$
$$\boldsymbol{R_B} = \frac{m_3\boldsymbol{r}_{q_3} + m_4\boldsymbol{r}_{\bar{q}_4}}{m_3+m_4},$$
$$\boldsymbol{R} = \boldsymbol{R_A} - \boldsymbol{R_B},$$
$$\boldsymbol{R_c} = \frac{m_1\boldsymbol{r}_{q_1} + m_2\boldsymbol{r}_{\bar{q}_2} + m_3\boldsymbol{r}_{q_3} + m_4\boldsymbol{r}_{\bar{q}_4}}{m_1+m_2+m_3+m_4}, \tag{16}$$

where the subscript $q/\bar{q}$ indicates the quark or antiquark particle, while the number indicates the quark position in

Fig. 2(a). As for the diquark-antidiquark configuration as shown in Fig. 2(b), the relevant Jacobi coordinates can be obtained by interchanging $\boldsymbol{r}_{q_3}$ with $\boldsymbol{r}_{\bar{q}_2}$ in Eq. (16).

Form the variational principle, after variation with respect to the relative motion wave function $\chi(R) = \sum_L \chi_L(R)$, one obtains the RGM equation, which is,

$$\int H(\boldsymbol{R},\boldsymbol{R}')\chi(\boldsymbol{R}')d\boldsymbol{R}' = E\int N(\boldsymbol{R},\boldsymbol{R}')\chi(\boldsymbol{R}')d\boldsymbol{R}', \quad (17)$$

where $H(\boldsymbol{R},\boldsymbol{R}')$ and $N(\boldsymbol{R},\boldsymbol{R}')$ are Hamiltonian and norm kernels, respectively. The eigenenergy E and the wave functions can be obtained by solving the RGM equation. In the present estimation, the function $\chi(\boldsymbol{R})$ can be expanded by Gaussian bases, which is

$$\chi(\boldsymbol{R}) = \frac{1}{\sqrt{4\pi}}\sum_L\left(\frac{1}{\pi b^2}\right)^{3/4}\sum_i^n C_{i,L} \times \int e^{-\frac{1}{2}(R-S_i)^2/b^2}Y^L(\hat{\boldsymbol{S}}_i)d\hat{\boldsymbol{S}}_i, \quad (18)$$

where $C_{i,L}$ is the expansion coefficient, and n is the number of gaussian bases, which is determined by the stability of the results. $\boldsymbol{S}_i$ is the separation of two reference centers. $\boldsymbol{R}$ is the dynamic coordinate defined in Eq. (16). After including the motion of the center of mass, i.e.,

$$\phi_C(\boldsymbol{R}_c) = \left(\frac{4}{\pi b^2}\right)^{3/4} e^{\frac{-2R_c^2}{b^2}}, \quad (19)$$

one can rewrite Eq. (13) as,

$$\psi_{4q} = \mathcal{A}\sum_{i,L} C_{i,L}\int\frac{d\hat{\boldsymbol{S}}_i}{\sqrt{4\pi}}\prod_{\alpha=1}^{2}\phi_\alpha(\boldsymbol{S}_i)\prod_{\alpha=3}^{4}\phi_\beta(-\boldsymbol{S}_i) \times [[\eta_{I_A S_A}\eta_{I_B S_B}]^{IS}Y^L(\hat{\boldsymbol{S}}_i)]^J[\chi_A^c\chi_B^c]^{[\sigma]}, \quad (20)$$

where $\phi_\alpha(\boldsymbol{S}_i)$ and $\phi_\beta(-\boldsymbol{S}_i)$ are the single-particle orbital wave functions with different reference centers, whose specific expressions have been presented in Eq. (11).

With the reformulated ansatz as shown in Eq. (20), the RGM equation becomes an algebraic eigenvalue equation, which is,

$$\sum_{j,L} C_{J,L}H_{i,j}^{L,L'} = E\sum_j C_{j,L'}N_{i,j}^{L'}, \quad (21)$$

where $N_{i,j}^{L'}$ and $H_{i,j}^{L,L'}$ are the overlap of the wave functions and the matrix elements of the Hamiltonian, respectively. By solving the generalized eigenvalue problem, we can obtain the energies of the tetraquark systems E and the corresponding expansion coefficients $C_{j,L}$. Finally, the relative motion wave function between two clusters can be obtained by substituting the $C_{j,L}$ into Eq. (18). In the resonating group method, with the increasing of the distance between two clusters, the continuum state will fall off toward its threshold, the energy of the bound state remains unchanged, while a resonance state is will tend to be stable. In this case, the fraction of kth-channel component of the resonance state can be estimated by $P_k = \frac{C_k^2}{C_1^2+C_2^2+C_3^2+\cdots C_n^2}$, where C_i indicates the corresponding coefficients for ith channel estimated by Eq. (21) in the channel coupling estimations.

As for the flavor, spin and color wave functions of the tetraquark system, they are constructed in a two step way. One can first construct the wave functions for the two clusters, and then coupling the wave functions of two clusters to form the wave function of tetraquark system. The details of the flavor, spin and color wave functions of tetraquark system are collected in the Appendix.

III. NUMERICAL RESULTS AND DISCUSSIONS

In this work, only the low-lying S–wave $T_{cc\bar{s}}$ tetraquark state are considered and the spin of the tetraquark system can be 0, 1, and 2. Thus, the spin parity of $T_{cc\bar{s}}$ tetraquark states can be 0^+, 1^+, and 2^+, respectively. Moreover, in the present estimations, both the meson-meson and diquark-antidiquark configurations are considered. In general, there are two types of color structures for the meson-meson configuration, which are color singlet-singlet $(\mathbf{1}_c \otimes \mathbf{1}_c)$ and the color octet-octet $(\mathbf{8}_c \otimes \mathbf{8}_c)$. The later color structures have been taken into account by the quark delocation, which is realized by constructing the single particle orbital wave function as a linear combination of the left and right Gaussians with a mixing parameter $\epsilon(s_i)$. The mixing indicates that there is a certain probability for the quarks between the two clusters to exchange. Thus in the QDCSM model, we only consider the color singlet-singlet structures. As for the diquark-antidiquark configuration, both the antitriplet-triplet $(\bar{\mathbf{3}}_c \otimes \mathbf{3}_c)$ and sextet-antisextet $(\mathbf{6}_c \otimes \bar{\mathbf{6}}_c)$ structure are taken into account. All the relevant channels for all possible quantum numbers are listed in Table II, where $F^i; S_s^j; \chi_k^c$ shows the necessary basis combinations in flavor (F^i), spin (S_s^j), and color (χ_k^c) degrees of freedom.

A. Bound state

With the above preparations, the low-lying S–wave $T_{cc\bar{s}}$ tetraquark states are systematically explored herein. In Tables III–V, we collect the estimated eigenenergies of the $T_{cc\bar{s}}$ tetraquark states with different J^P quantum numbers. In those tables, the index of the first column represents the symbols of each channel and in the second and third columns we list all the involved channels and the corresponding theoretical threshold, respectively. Moreover, E_{sc} is the eigenenergy obtained in the single channel estimations, E_{cc} and $E_{\rm mix}$ are the eigenenergies estimated by considering the coupled channel effects in

TABLE II. The relevant channels for all possible J^P quantum numbers.

$J^P = 0^+$			$J^P = 1^+$			$J^P = 2^+$		
Index	$F^i; S_s^j; \chi_k^c$ [i; j; k]	Channels	Index	$F^i; S_s^j; \chi_k^c$ [i; j; k]	Channels	Index	$F^i; S_s^j; \chi_k^c$ [i; j; k]	Channels
1	[1,1,1]	$D^0 D_s^+$	1	[1,3,1]	$D^0 D_s^{*+}$	1	[1,6,1]	$D^* D_s^{*+}$
2	[1,2,1]	$D^* D_s^{*+}$	2	[1,4,1]	$D^* D_s^+$	2	[2,6,4]	$(cc)(\bar{q}\,\bar{s})$
3	[2,1,3]	$(cc)(\bar{q}\,\bar{s})$	3	[1,5,1]	$D^* D_s^{*+}$			
4	[2,2,4]	$(cc)(\bar{q}\,\bar{s})$	4	[2,3,3]	$(cc)(\bar{q}\,\bar{s})$			
			5	[2,4,4]	$(cc)(\bar{q}\,\bar{s})$			
			6	[2,5,4]	$(cc)(\bar{q}\,\bar{s})$			

TABLE III. The low-lying eigenenergies (in unit of MeV) of $T_{cc\bar{s}}$ tetraquark states with $J^P = 0^+$.

			QDCSM1			QDCSM2			QDCSM3		
Index	Channel	Threshold	E_{sc}	E_{cc}	$E_{\rm mix}$	E_{sc}	E_{cc}	$E_{\rm mix}$	E_{sc}	E_{cc}	$E_{\rm mix}$
1	$D^0 D_s^+$	3833	3836.3	3836.2	3836.2	3836.3	3836.3	3836.2	3836.2	3836.2	3836.2
2	$D^* D_s^{*+}$	4119	4119.7			4120.9			4121.2		
3	$(cc)(\bar{q}\,\bar{s})$		4589.3	4299.8		4585.1	4291.8		4574.7	4277.9	
4	$(cc)(\bar{q}\,\bar{s})$		4321.3			4316.5			4308.0		

TABLE IV. The same as Table III but for the tetraquark states with $J^P = 1^+$.

			QDCSM1			QDCSM2			QDCSM3		
Index	Channel	Threshold	E_{sc}	E_{cc}	$E_{\rm mix}$	E_{sc}	E_{cc}	$E_{\rm mix}$	E_{sc}	E_{cc}	$E_{\rm mix}$
1	$D^0 D_s^{*+}$	3977	3978.2	3977.1	3971.1	3978.2	3977.7	3973.8	3978.2	3978.1	3974.8
2	$D^* D_s^+$	3975	3978.0			3978.1			3978.2		
3	$D^* D_s^{*+}$	4119	4110.8			4117.2			4118.1		
4	$(cc)(\bar{q}\,\bar{s})$		4544.2	4128.2		4535.4	4127.2		4518.9	4124.1	
5	$(cc)(\bar{q}\,\bar{s})$		4132.7			4132.5			4130.7		
6	$(cc)(\bar{q}\,\bar{s})$		4337.5			4334.1			4327.8		

TABLE V. The same as Table III but for the tetraquark states with $J^P = 2^+$.

			QDCSM1			QDCSM2			QDCSM3		
Index	Channel	Threshold	E_{sc}	E_{cc}	$E_{\rm mix}$	E_{sc}	E_{cc}	$E_{\rm mix}$	E_{sc}	E_{cc}	$E_{\rm mix}$
1	$D^* D_s^{*+}$	4119	4122.0	⋯	4121.5	4122.2	⋯	4122.1	4122.3	⋯	4122.2
2	$(cc)(\bar{q}\,\bar{s})$		4367.1	⋯		4366.3	⋯		4364.1	⋯	

each kind of configuration, and in both configurations, respectively.

Additionally, we define the binding energy E_b of the $T_{cc\bar{s}}$ tetraquark states as $E_{bi} = E_i - E_4(\infty)$ to identify whether or not the tetraquark states are stable against the strong interactions, where $E_4(\infty)$ is the lowest possible threshold of the two meson structure estimated in the QDCSM. and i represents the different situation of channel coupling. Such a subtraction procedure can greatly reduce the influence of the model parameters on the binding energies. If $E_b > 0$, the tetraqaurk systems can fall apart into two mesons via the strong interactions. If $E_b < 0$, the strong decay into two mesons is forbidden kinemetically and therefore the decay can only occur via either the weak or electromagnetic interaction.

For the $T_{cc\bar{s}}$ tetraquark system with $J^P = 0^+$, there are two channels in the meson-configuration and two channels in the diquark-antidiquark configuration. The estimated eigenenergies of $T_{cc\bar{s}}$ state with $J^P = 0^+$ are listed in Table III. The theoretical thresholds of the meson-meson channels are also presented for comparison. With the parameters in QDCSM1, the single channel estimations in

the meson-meson configuration find that the eigenenergies are all above the corresponding threshold, which indicate that the single channel estimations do not support the existence of the bound states. In addition, when considering the coupled channels effects in the meson-meson configurations, we find the estimated eigenenergy is 3836.2 MeV, which is above the threshold of $D^0D_s^+$. The lowest eigenenergy obtained by coupled channel estimations in the meson-meson configuration is very close to the one of the single channel estimations in the $D^0D_s^+$ channel, which indicates that the coupled channel effect in the meson-meson configuration is rather weak. As for the diquark-antidiquark configuration, both the single channel estimations and the coupled channel estimations indicate that the eigenenergies are above the threshold of $D^0D_s^+$. Different from the meson-meson configuration, we find the eigenenergy obtained from the coupled channel estimation is at least 20 MeV below the lowest one of the single channel estimation, which indicate the coupled channels effect in the diquark-antidiquark configuration is much strong. Moreover, we extend the coupled channel effect in both configurations, and the eigenenergy is estimated to be 3836.2 MeV, which is still above the threshold of $D^0D_s^+$. The results estimated with the parameters in QDCSM2 and QDCSM3 are very similar with those obtained with the parameter in QDCSM1 and no stable tetraquark state is found.

For the $T_{cc\bar{s}}$ tetraquark system with $J^P = 1^+$, there are six channels, including three channels in the meson-meson configuration and three channels in the diquark-antidiquark configuration. From Table IV, the estimated results of three sets of model parameters are almost identical. When considering the single channel estimations in the meson-meson configuration, we find that the estimated eigenenergy of $D^0D_s^{*+}$ and $D^*D_s^+$ channels are above the theoretical threshold of the corresponding physical channels, which indicates that these channels are scattering channels in single channel calculations. However, a bound state in the $D^*D_s^{*+}$ channel with the bound energy about 1–10 MeV is obtained with all three sets of model parameters. Besides, by the coupling channels with the meson-meson configuration, the estimated eigenenergy is slightly above the lowest theoretical threshold of the $D^*D_s^+$, which show that the effect of couple channels in the meson-meson configuration is rather weak. For the diquark-antidiquark configuration, the estimated eigenenergies obtained for the single-channel and channel-coupled estimations are above the theoretical threshold of the lowest channel $D^*D_s^+$. Nevertheless, when the channel coupling between the two configuration are taken into account, a shallow bound state is detected, although the magnitude of the bound energy is slightly different with different sets of the model parameters.

In view of the above conclusions, we estimate the average values of each terms in the Hamiltonian to examine how a shallow $D^*D_s^+$ bound state with $J^P = 1^+$ is created. In Table VI, we present the individual contributions to E_b from the kinetic energy term, and the interaction potential terms, respectively. In addition, the average values of each term for two conventional D^* and D_s^+ mesons without interactions, i.e., the distance between the two mesons are large enough, are also listed in the table for comparison. Here, we define $\Delta E_{sc} = E_{sc} - E_4$, $\Delta E_{cc} = E_{cc} - E_4$, and $\Delta E_{\rm mix} = E_{\rm mix} - E_4$. From our estimations, we find the contributions from the confinement potential are always positive, which indicate that confinement potential provides repulsive forces that prevent from the bounding two mesons as a tetraquark state. For the kinetic energy term, with more physical channels taking into consideration, the properties of kinetic energy basically transforms gradually from repulsion toward very strong attraction for QDCSM1 and QDCSM2, while for QDCSM3, the repulsive interaction resulted from the kinetic energy term becomes weak with more channels involved. Similar tendency appear in the one-gluon-exchange interaction. Thus, the present estimations imply that the kinetic term and the one-gluon-exchange interaction favor of forming a tetraqurk states rather than two individual mesons. Such a phenomenon illustrates the very delicate competition between the

TABLE VI. Contributions of each terms in Hamiltonian to the energy of the $D^0D_s^{*+}$ bound state with $J^P = 1^+$ in unit of MeV. E_4 stands for the lowest possible threshold of two mesons estimated in QDCSM. Our estimations indicate the contributions of η meson exchange potential are all less than 0.05 MeV in different sets of model parameters. Thus, the contributions from η meson exchange are not presented.

	QDCSM1				QDCSM2				QDCSM3			
	H_T	$V_{\rm CON}$	$V_{\rm OGE}$	V_K	H_T	$V_{\rm CON}$	$V_{\rm OGE}$	V_K	H_T	$V_{\rm CON}$	$V_{\rm OGE}$	V_K
E_{sc}	1081.3	−901.7	−506.6	∼0.0	1011.2	−783.9	−554.2	∼0.0	917.9	−615.9	−628.8	∼0.0
E_{cc}	1073.9	−895.9	−505.8	−0.1	1008.8	−782.5	−553.5	−0.1	917.1	−615.5	−628.5	∼0.0
$E_{\rm mix}$	1049.0	−820.4	−558.1	−4.4	998.4	−752.4	−573.7	−3.5	915.3	−609.8	−635.4	−0.3
E_4	1079.6	−903.3	−506.1	∼0.0	1008.7	−784.7	−553.8	∼0.0	915.0	−616.3	−628.5	∼0.0
ΔE_{sc}	1.7	1.6	−0.5	∼0.0	2.5	0.8	0.4	∼0.0	2.9	0.4	−0.3	∼0.0
ΔE_{cc}	−5.7	7.4	0.3	−0.1	0.1	2.2	−0.3	−0.1	2.1	0.8	0.0	∼0.0
$\Delta E_{\rm mix}$	−30.6	82.9	−52.0	−4.4	−10.3	32.3	−19.9	−3.5	0.3	5.5	−7.2	−0.3

kinetic energy and the interaction potential from various sources in the Hamiltonian.

For the $T_{cc\bar{s}}$ tetraquark system with $J^P = 2^+$, only one physics channel in the meson-meson configuration and one channel in the diquark-antidiquark configuration exists. From Table V, one can find the eigenenergies obtained from the single channel estimation is higher than the physical meson-meson channel. After considering the coupled channel effect between the meson-meson and diquark-antidiquark configurations, the estimated eigenenergy is still above the threshold of $D^*D_s^{*+}$, which indicates that there is no bound state in the $T_{cc\bar{s}}$ tetraquark system with $J^P = 2^+$.

B. Resonance states

In the bound state estimations, we find one bound state with $J^P = 1^+$ while there is no bound state in the $J^P = 0^+$ and $J^P = 2^+$ systems. In the following, we will employ the real scaling method to explore the possible resonance states in the $T_{cc\bar{s}}$ tetraquark system. To determine whether these resonance states could be detected by the open channels, we perform a channel coupling estimation by including all the meson-meson and diquark-antidiquark channels in the estimations.

The real scaling method is developed to identify the genuine resonances from the states with discrete energies with finite volume [86]. In this method, a factor $\mathbf{S}_m$, which is the distance between two clusters, is adopted to scale the finite volume. So with the increase of the distance between two clusters, the continuum state will fall off toward its threshold, the energy of the bound state remains unchanged, while a resonance state will tend to be stable. If the energy of a scattering state is far away from the one of the resonance, the coupling between the resonance and the scattering states is rather weak, and the energy of the resonance is almost stable. When the energy of the scattering state approaches the one of the resonance due to the increasing of $\mathbf{S}_m$, the coupling will become strong, and if $\mathbf{S}_m$ increases further, the energy gap between the resonance and scattering states will increase and the coupling will become weak again. In this way, an avoided crossing structure appears. This is a general feature of two interacting energy levels. Because of the continuum nature of the scattering states, the avoided crossing structure will show up repeatedly with the increasing of $\mathbf{S}_m$ as shown in Fig. 3 and the resonance line corresponds to the energy of the resonance state. In addition, from the slopes of resonance and scattering states, the decay width can be estimated by,

$$\Gamma = 4|V_{\min}(S)|\frac{\sqrt{|k_r||k_c|}}{|k_r - k_c|}, \tag{22}$$

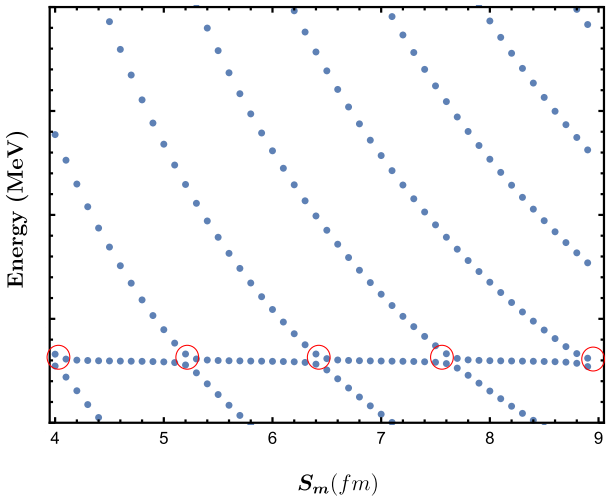

FIG. 3. A sketch diagram of the resonance shape in the real-scaling method.

where k_r and k_c are the slopes of the resonance and scattering states, respectively. While, $V_{\min}(S)$ is the minimal energy difference between the resonance and the scattering state at avoided crossing point. This method has been successfully applied to investigate the pentaquark [87,88], the dibaryon [84], and the tetraquark systems [79,89,90].

In the present work, we expand the spacial wave function with a set of Gaussians with differences $\mathbf{S}_m$, $(m = 1, 2, 3, \ldots, n)$ and the distance with the relative motion of two clusters can be scaled. So we calculate the energy eigenvalues of the $T_{cc\bar{s}}$ tetraquark system by taking the value of the largest distance (S_m) between two clusters from 4.0 to 9.0 fm to check if there is any resonance state. Here, we take the results of the QDCSM1 as examples, which are shown in Fig. 4 with different J^P quantum numbers. For the $T_{cc\bar{s}}$ tetraquark system with $J^P = 0^+$ as shown in Fig. 4(a), one can note that the lower black horizontal line corresponds to the physical threshold of $D_s^+D^0$, while the upper blue horizontal line with the energy to be about 4114 MeV, locates below the threshold of $D^*D_s^{+*}$, which corresponds to a resonance state since the resonance behavior appearing in the Fig. 4(a) as the finite space is constantly expanding. Moreover, the resonance state is estimated by considering the full channel coupling, and the present result indicates that its main ingredient is $D^*D_s^{+*}$. In other words, the effect of the channel coupling push the energy of the physical channel $D^*D_s^{+*}$ a bit below its threshold. In addition, the width of this resonance state is estimated to be about 14.3 MeV according to Eq. (22).

For the $T_{cc\bar{s}}$ tetraquark system with $J^P = 1^+$ as shown in Fig. 4(b), it is obvious that the lowest red horizontal line locates at the energy of 3971 MeV, which is below the

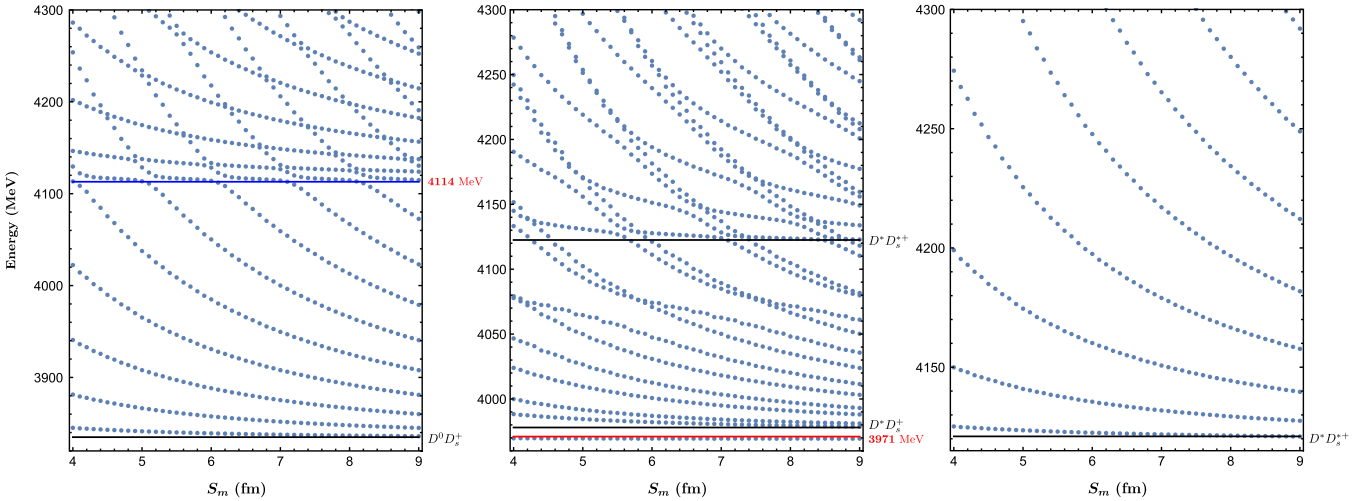

FIG. 4. The stabilization plots of the energies of the $T_{cc\bar{s}}$ tetraquark systems.

threshold of the $D^0D_s^{+*}$, and this represents the bound states of $T_{cc\bar{s}}$ tetraquark system with $J^P = 1^+$. This conclusion is consistent with the estimations in the last subsection. Moreover, two additional horizontal lines are also presented, which stand for the threshold of $D^*D_s^+$ and $D^*D_s^{*+}$, respectively. The present estimations indicate that there is no resonance state in the $T_{cc\bar{s}}$ tetraquark system with $J^P = 1^+$, and the bound state in the $D^*D_s^{*+}$ channel becomes the scattering state by the effect of the channel coupling. For the $T_{cc\bar{s}}$ tetraquark system with $J^P = 2^+$ as shown in Fig. 4(c), there is one horizontal line, which represents the threshold of $D^*D_s^{*+}$. It is clearly to conclude that there are no bound or resonant states in the $T_{cc\bar{s}}$ tetraquark system with $J^P = 2^+$.

In addition, we perform the same estimations for the $T_{cc\bar{s}}$ tetraquark system in the QDCSM2 and QDCSM3. The results are similar to those of QDCSM1. We summarize the results obtained from three sets of model parameters in Table VII. By taking the coupled channel effects into consideration, we find one resonance state with a mass 4113–4114 MeV for the $T_{cc\bar{s}}$ tetraquark system with $J^P = 0^+$. The dominant component of the resonance state is $D^*D_s^{*+}$ with the percentage of this component to be about 80%. Moreover, the decay width of this resonance state is predicted to be 14.3–16.1 MeV. For the $J^P = 1^+$ system, there is a bound state with energy range (3971.1–3974.8) MeV and no resonance state is obtained. For the $T_{cc\bar{s}}$ tetraquark system with $J^P = 2^+$, no resonance or bound state is obtained by the channel coupling estimations.

TABLE VII. The energies and widths of the $T_{cc\bar{s}}$ tertraquark states.

State		Parameter sets		
	J^P	QDCSM1	QDCSM2	QDCSM3
Bound	1^+	3971.1	3973.8	3974.8
Resonance	0^+	4114/14.3	4114/15.8	4113/16.1

IV. SUMMARY

In the present work, the $T_{cc\bar{s}}$ tetraquark system with the quantum number $J^P = 0^+, 1^+, 2^+$ are systemically investigated to search for the possible bound state and resonance state by using the RGM in the QDCSM framework. In the model, both meson-meson and diquark-antidiquark configurations are taken into account, and the single-channel and the coupled channel calculations are preformed to obtain the energy of the $T_{cc\bar{s}}$ tetraquark system. In addition, a stabilization calculation is carried out to seek for possible resonance states. Furthermore, to check whether the estimated results are parameter dependent, three different sets of model parameters are employed in the calculation and we find the qualitative results of three sets of model parameters for the $T_{cc\bar{s}}$ tetraquark system are very similar.

From the present estimations, we find that the coupled channel effects plays important role in the $T_{cc\bar{s}}$ tetraquark system. After taking the coupled channel effects into consideration, we predict one bound state with the energy to be 3971.1–3974.8 MeV and $J^P = 1^+$. Moreover, one resonance state with $J^P = 0^+$ is also obtained, the resonance mass and width are estimated to be 4113–4114 MeV and 14.3–16.1 MeV, respectively. The predictions in the present work could be experimentally detected in the future by LHCb and Belle II. Additionally the theoretical and further experimental investigations for properties of the $T_{cc\bar{s}}$ tetraquark could pave the way for possible doubly and triply tetraquark states.

ACKNOWLEDGMENTS

This work is supported partly by the National Natural Science Foundation of China under Contract No. 12175037, No. 12335001, No. 11775118 and No. 11535005. This work is also supported by China Postdoctoral Science Foundation funded Projects No. 2021M690626, and No. 1107020201.

APPENDIX: THE WAVE FUNCTION OF THE OPEN HEAVY CHARM TETRAQUARK WITH STRANGENESS

1. The color wave function

Plenty of color structures in multiquark systems will be available with respect to those of conventional hadrons such as $q\bar{q}$ mesons and qqq baryons. In this appendix, we present how to construct the colorless wave function for a tetraquark system.

For the meson-meson configurations, the color wave functions of a $q\bar{q}$ cluster would be,

$$\begin{aligned}
C^1_{[111]} &= \sqrt{\frac{1}{3}}(r\bar{r}+g\bar{g}+b\bar{b}),\\
C^2_{[21]} &= r\bar{b}, \qquad C^3_{[21]} = -r\bar{g},\\
C^4_{[21]} &= g\bar{b}, \qquad C^5_{[21]} = -b\bar{g},\\
C^6_{[21]} &= g\bar{r}, \qquad C^7_{[21]} = b\bar{r},\\
C^8_{[21]} &= \sqrt{\frac{1}{2}}(r\bar{r}-g\bar{g}),\\
C^9_{[21]} &= \sqrt{\frac{1}{6}}(-r\bar{r}-g\bar{g}+2b\bar{b}),
\end{aligned} \tag{A1}$$

where the subscript [111] and [21] stand for color-singlet ($\mathbf{1}_c$) and color-octet ($\mathbf{8}_c$), respectively. So, the $\mathrm{SU}(3)_{\mathrm{color}}$ wave functions of color-singlet (two color-singlet clusters, $\mathbf{1}_c \otimes \mathbf{1}_c$) and hidden-color (two color-octet clusters, $\mathbf{8}_c \otimes \mathbf{8}_c$) channels are given, respectively,

$$\begin{aligned}
\chi^c_1 &= C^1_{[111]}C^1_{[111]},\\
\chi^c_2 &= \sqrt{\frac{1}{8}}\Big(C^2_{[21]}C^7_{[21]} - C^4_{[21]}C^5_{[21]} - C^3_{[21]}C^6_{[21]}\\
&\quad + C^8_{[21]}C^8_{[21]} - C^6_{[21]}C^3_{[21]} + C^9_{[21]}C^9_{[21]}\\
&\quad - C^5_{[21]}C^4_{[21]} + C^7_{[21]}C^2_{[21]}\Big).
\end{aligned} \tag{A2}$$

For the diquark-antidiquark structure, the color wave functions of the diquark clusters are,

$$\begin{aligned}
C^1_{[2]} &= rr, \qquad C^2_{[2]} = \sqrt{\frac{1}{2}}(rg+gr),\\
C^3_{[2]} &= gg, \qquad C^4_{[2]} = \sqrt{\frac{1}{2}}(rb+br),\\
C^5_{[2]} &= \sqrt{\frac{1}{2}}(gb+bg), \qquad C^6_{[2]} = bb,\\
C^7_{[11]} &= \sqrt{\frac{1}{2}}(rg-gr), \qquad C^8_{[11]} = \sqrt{\frac{1}{2}}(rb-br),\\
C^9_{[11]} &= \sqrt{\frac{1}{2}}(gb-bg).
\end{aligned} \tag{A3}$$

While the color wave functions of the antidiquark clusters can be written as,

$$\begin{aligned}
C^1_{[22]} &= \bar{r}\,\bar{r}, \qquad C^2_{[22]} = -\sqrt{\frac{1}{2}}(\bar{r}\,\bar{g}+\bar{g}\,\bar{r}),\\
C^3_{[22]} &= \bar{g}\,\bar{g}, \qquad C^4_{[22]} = \sqrt{\frac{1}{2}}(\bar{r}\,\bar{b}+\bar{b}\,\bar{r}),\\
C^5_{[22]} &= -\sqrt{\frac{1}{2}}(\bar{g}\,\bar{b}+\bar{b}\,\bar{g}), \qquad C^6_{[22]} = \bar{b}\,\bar{b},\\
C^7_{[211]} &= \sqrt{\frac{1}{2}}(\bar{r}\,\bar{g}-\bar{g}\,\bar{r}), \qquad C^8_{[211]} = -\sqrt{\frac{1}{2}}(\bar{r}\,\bar{b}-\bar{b}\,\bar{r}),\\
C^9_{[211]} &= \sqrt{\frac{1}{2}}(\bar{g}\,\bar{b}-\bar{b}\,\bar{g}).
\end{aligned} \tag{A4}$$

The color-singlet wave functions of the diquark-antidiquark configuration can be the product of color sextet and antisextet clusters ($\mathbf{6}_c \otimes \bar{\mathbf{6}}_c$) or the product of color-triplet and antitriplet cluster ($\mathbf{3}_c \otimes \bar{\mathbf{3}}_c$), which read,

$$\begin{aligned}
\chi^c_3 &= \sqrt{\frac{1}{6}}\Big(C^1_{[2]}C^1_{[22]} - C^2_{[2]}C^{[2]}_{[22]} + C^3_{[2]}C^3_{[22]}\\
&\quad + C^4_{[2]}C^4_{[22]} - C^5_{[2]}C^5_{[22]} + C^6_2C^6_{22}\Big),\\
\chi^c_4 &= \sqrt{\frac{1}{3}}\Big(C^7_{[11]}C^7_{[211]} - C^8_{[11]}C^8_{[211]} + C^9_{[11]}C^9_{[211]}\Big).
\end{aligned} \tag{A5}$$

2. The flavor wave function

For the flavor degree of freedom, the different coupling methods generate different flavor wave function. From the Table II, the $T_{cc\bar{s}}$ tetraquark flavor wave function can be categorized as F^i_m and F^i_d, where the subscript m and d refer to meson-meson and the diquark-antidiquark configurations, respectively. Distinctive structures are gotten the quark coupling arrange. For the meson-meson structure, the coupling orders can be accessed as,

$$F_m^1 = (c\bar{q}) - (c\bar{s}), \tag{A6}$$

while for the diquark-antidiquark structure, the flavor wave function should be written as

$$F_d^2 = (cc) - (\bar{q}\,\bar{s}) \tag{A7}$$

3. The spin wave function

The total spin S of tetraquark states ranges from 0 to 2. All of them are considered. The wave functions of two body clusters are,

$$\begin{aligned}\chi_{11} &= \alpha\alpha,\\ \chi_{10} &= \sqrt{\frac{1}{2}}(\alpha\beta + \beta\alpha),\\ \chi_{1-1} &= \beta\beta,\\ \chi_{00} &= \sqrt{\frac{1}{2}}(\alpha\beta - \beta\alpha).\end{aligned} \tag{A8}$$

Then, the total spin wave functions S_s^i are obtained by considering the coupling of two subcluster spin wave functions with SU(2) algebra, and the total spin wave functions of four-quark states can be read as,

$$\begin{aligned}S_0^1 &= \chi_{00}\chi_{00},\\ S_0^2 &= \sqrt{\frac{1}{3}}(\chi_{11}\chi_{1-1} - \chi_{10}\chi_{10} + \chi_{1-1}\chi_{11}),\\ S_1^3 &= \chi_{00}\chi_{11},\\ S_1^4 &= \chi_{11}\chi_{00},\\ S_1^5 &= \sqrt{\frac{1}{2}}(\chi_{11}\chi_{10} - \chi_{10}\chi_{11}),\\ S_2^6 &= \chi_{11}\chi_{11}.\end{aligned} \tag{A9}$$

[1] M. Ablikim *et al.* (BESIII Collaboration), Phys. Rev. Lett. **110**, 252001 (2013).
[2] Z. Q. Liu *et al.* (Belle Collaboration), Phys. Rev. Lett. **110**, 252002 (2013); **111**, 019901(E) (2013).
[3] T. Xiao, S. Dobbs, A. Tomaradze, and K. K. Seth, Phys. Lett. B **727**, 366 (2013).
[4] M. Ablikim *et al.* (BESIII Collaboration), Phys. Rev. Lett. **119**, 072001 (2017).
[5] S. S. Agaev, K. Azizi, and H. Sundu, Phys. Rev. D **93**, 074002 (2016).
[6] J. M. Dias, F. S. Navarra, M. Nielsen, and C. M. Zanetti, Phys. Rev. D **88**, 016004 (2013).
[7] Z. G. Wang and T. Huang, Phys. Rev. D **89**, 054019 (2014).
[8] C. Deng, J. Ping, and F. Wang, Phys. Rev. D **90**, 054009 (2014).
[9] Z. G. Wang and T. Huang, Eur. Phys. J. C **74**, 2891 (2014).
[10] E. Wilbring, H. W. Hammer, and U. G. Meißner, Phys. Lett. B **726**, 326 (2013).
[11] Y. Dong, A. Faessler, T. Gutsche, and V. E. Lyubovitskij, Phys. Rev. D **88**, 014030 (2013).
[12] H. W. Ke, Z. T. Wei, and X. Q. Li, Eur. Phys. J. C **73**, 2561 (2013).
[13] T. Gutsche, M. Kesenheimer, and V. E. Lyubovitskij, Phys. Rev. D **90**, 094013 (2014).
[14] A. Esposito, A. L. Guerrieri, and A. Pilloni, Phys. Lett. B **746**, 194 (2015).
[15] D. Y. Chen and Y. B. Dong, Phys. Rev. D **93**, 014003 (2016).
[16] Q. R. Gong, Z. H. Guo, C. Meng, G. Y. Tang, Y. F. Wang, and H. Q. Zheng, Phys. Rev. D **94**, 114019 (2016).
[17] H. W. Ke and X. Q. Li, Eur. Phys. J. C **76**, 334 (2016).
[18] E. S. Swanson, Phys. Rev. D **91**, 034009 (2015).
[19] Y. Ikeda, S. Aoki, T. Doi, S. Gongyo, T. Hatsuda, T. Inoue, T. Iritani, N. Ishii, K. Murano, and K. Sasaki (HAL QCD Collaboration), Phys. Rev. Lett. **117**, 242001 (2016).
[20] A. P. Szczepaniak, Phys. Lett. B **747**, 410 (2015).
[21] D. Y. Chen and X. Liu, Phys. Rev. D **84**, 034032 (2011).
[22] D. Y. Chen, X. Liu, and T. Matsuki, Phys. Rev. D **88**, 036008 (2013).
[23] E. S. Swanson, Int. J. Mod. Phys. E **25**, 1642010 (2016).
[24] D. Ebert, R. N. Faustov, and V. O. Galkin, Eur. Phys. J. C **58**, 399 (2008).
[25] J. Ferretti and E. Santopinto, J. High Energy Phys. 04 (2020) 119.
[26] S. H. Lee, M. Nielsen, and U. Wiedner, J. Korean Phys. Soc. **55**, 424 (2009).
[27] J. M. Dias, X. Liu, and M. Nielsen, Phys. Rev. D **88**, 096014 (2013).
[28] D. Y. Chen, X. Liu, and T. Matsuki, Phys. Rev. Lett. **110**, 232001 (2013).
[29] M. Ablikim *et al.* (BESIII Collaboration), Phys. Rev. Lett. **126**, 102001 (2021).
[30] R. Aaij *et al.* (LHCb Collaboration), Phys. Rev. Lett. **127**, 082001 (2021).
[31] H. X. Chen, Phys. Rev. D **105**, 094003 (2022).

[32] B. D. Wan and C. F. Qiao, Nucl. Phys. **B968**, 115450 (2021).
[33] Y. J. Xu, Y. L. Liu, C. Y. Cui, and M. Q. Huang, Phys. Rev. D **104**, 094028 (2021).
[34] R. M. Albuquerque, S. Narison, and D. Rabetiarivony, Phys. Rev. D **103**, 074015 (2021).
[35] U. Özdem and K. Azizi, Eur. Phys. J. Plus **136**, 968 (2021).
[36] U. Özdem and A. K. Yıldırım, Phys. Rev. D **104**, 054017 (2021).
[37] Q. N. Wang, W. Chen, and H. X. Chen, Chin. Phys. C **45**, 093102 (2021).
[38] L. Meng, B. Wang, and S. L. Zhu, Phys. Rev. D **102**, 111502 (2020).
[39] Z. Yang, X. Cao, F. K. Guo, J. Nieves, and M. P. Valderrama, Phys. Rev. D **103**, 074029 (2021).
[40] M. C. Du, Q. Wang, and Q. Zhao, arXiv:2011.09225.
[41] L. Maiani, A. D. Polosa, and V. Riquer, Sci. Bull. **66**, 1616 (2021).
[42] P. P. Shi, F. Huang, and W. L. Wang, Phys. Rev. D **103**, 094038 (2021).
[43] J. F. Giron, R. F. Lebed, and S. R. Martinez, Phys. Rev. D **104**, 054001 (2021).
[44] R. Chen, Q. Huang, X. Liu, and S. L. Zhu, Phys. Rev. D **104**, 114042 (2021).
[45] A. Feijoo, W. H. Liang, and E. Oset, Phys. Rev. D **104**, 114015 (2021).
[46] F. L. Wang and X. Liu, Phys. Rev. D **104**, 094030 (2021).
[47] F. L. Wang, R. Chen, and X. Liu, Phys. Lett. B **835**, 137502 (2022).
[48] H. Ren, F. Wu, and R. Zhu, Adv. High Energy Phys. **2022**, 9103031 (2022).
[49] Q. Xin and Z. G. Wang, Eur. Phys. J. A **58**, 110 (2022).
[50] K. Azizi and U. Özdem, Phys. Rev. D **104**, 114002 (2021).
[51] U. Özdem, Phys. Rev. D **105**, 054019 (2022).
[52] M. Albaladejo, Phys. Lett. B **829**, 137052 (2022).
[53] L. R. Dai, E. Oset, A. Feijoo, R. Molina, L. Roca, A. M. Torres, and K. P. Khemchandani, Phys. Rev. D **105**, 074017 (2022).
[54] M. L. Du, V. Baru, X. K. Dong, A. Filin, F. K. Guo, C. Hanhart, A. Nefediev, J. Nieves, and Q. Wang, Phys. Rev. D **105**, 014024 (2022).
[55] M. J. Zhao, Z. Y. Wang, C. Wang, and X. H. Guo, Phys. Rev. D **105**, 096016 (2022).
[56] H. W. Ke, X. H. Liu, and X. Q. Li, Eur. Phys. J. C **82**, 144 (2022).
[57] X. Chen and Y. Yang, Chin. Phys. C **46**, 054103 (2022).
[58] N. Santowsky and C. S. Fischer, Eur. Phys. J. C **82**, 313 (2022).
[59] C. Deng and S. L. Zhu, Phys. Rev. D **105**, 054015 (2022).
[60] L. R. Dai, R. Molina, and E. Oset, Phys. Rev. D **105**, 016029 (2022).
[61] T. Guo, J. Li, J. Zhao, and L. He, Phys. Rev. D **105**, 014021 (2022).
[62] X. Z. Weng, W. Z. Deng, and S. L. Zhu, Chin. Phys. C **46**, 013102 (2022).
[63] S. S. Agaev, K. Azizi, and H. Sundu, Nucl. Phys. **B975**, 115650 (2022).
[64] R. Aaij *et al.* (LHCb Collaboration), Nat. Phys. **18**, 751 (2022).
[65] R. Aaij *et al.* (LHCb Collaboration), Nat. Commun. **13**, 3351 (2022).
[66] P. Junnarkar, N. Mathur, and M. Padmanath, Phys. Rev. D **99**, 034507 (2019).
[67] E. J. Eichten and C. Quigg, Phys. Rev. Lett. **119**, 202002 (2017).
[68] S. Q. Luo, K. Chen, X. Liu, Y. R. Liu, and S. L. Zhu, Eur. Phys. J. C **77**, 709 (2017).
[69] M. Karliner and J. L. Rosner, Phys. Rev. D **105**, 034020 (2022).
[70] A. De Rujula, H. Georgi, and S. L. Glashow, Phys. Rev. D **12**, 147 (1975).
[71] N. Isgur and G. Karl, Phys. Rev. D **18**, 4187 (1978).
[72] N. Isgur and G. Karl, Phys. Rev. D **19**, 2653 (1979); **23**, 817 (E) (1981).
[73] N. Isgur and G. Karl, Phys. Rev. D **20**, 1191 (1979).
[74] M. Chen, H. Huang, J. Ping, and F. Wang, Phys. Rev. C **83**, 015202 (2011).
[75] J. L. Ping, F. Wang, G. H. Wu, L. J. Teng, and J. T. Goldman, Nucl. Phys. **A688**, 871 (2001).
[76] F. Wang, D. Qing, P. Xu, and J. L. Ping, Nucl. Phys. **A631**, 462C (1998).
[77] H. Huang, C. Deng, J. Ping, and F. Wang, Eur. Phys. J. C **76**, 624 (2016).
[78] M. Tanabashi *et al.* (Particle Data Group), Phys. Rev. D **98**, 030001 (2018).
[79] X. Liu, H. Huang, J. Ping, D. Chen, and X. Zhu, Eur. Phys. J. C **81**, 950 (2021).
[80] L. Chen, H. Pang, H. Huang, J. Ping, and F. Wang, Phys. Rev. C **76**, 014001 (2007).
[81] M. Xu, M. Yu, and L. Liu, Phys. Rev. Lett. **100**, 092301 (2008).
[82] H. Huang, P. Xu, J. Ping, and F. Wang, Phys. Rev. C **84**, 064001 (2011).
[83] H. Huang, J. Ping, X. Zhu, and F. Wang, Eur. Phys. J. C **82**, 805 (2022).
[84] Z. Xia, S. Fan, X. Zhu, H. Huang, and J. Ping, Phys. Rev. C **105**, 025201 (2022).
[85] M. Kamimura, Nucl. Phys. **A351**, 456 (1981).
[86] J. Simon, J. Chem. Phys. **75**, 2465 (1981).
[87] E. Hiyama, M. Kamimura, A. Hosaka, H. Toki, and M. Yahiro, Phys. Lett. B **633**, 237 (2006).
[88] E. Hiyama, A. Hosaka, M. Oka, and J. M. Richard, Phys. Rev. C **98**, 045208 (2018).
[89] X. Liu, D. Chen, H. Huang, J. Ping, X. Chen, and Y. Yang, Sci. China Phys. Mech. Astron. **66**, 221012 (2023).
[90] X. Jin, Y. Y. Xue, H. X. Huang, and J. L. Ping, Eur. Phys. J. C **80**, 1083 (2020).